2013 IEEE/RSJ International Conference on
Intelligent Robots and Systems (IROS)
November 3-7, 2013. Tokyo, Japan

MEMS-based State Feedback Control of Multi-Body Hydraulic Manipulator

Janne Honkakorpi[1], Juho Vihonen[2] and Jouni Mattila[1]

Abstract— **This paper presents closed-loop state feedback motion control of a heavy-duty hydraulic manipulator using solely micro-electro-mechanical systems (MEMS) rate gyroscopes and linear accelerometers for joint angular position, velocity and acceleration feedback. For benchmarking, incremental encoders with 2 million counts per revolution are also used to supply the joint motion state feedback. The two motion state estimation methods are compared using Cartesian path trajectory closed-loop control experiments with both position feedback-based proportional control and motion state-based feedback control. The experiments show that the proposed MEMS-based state feedback control yields comparable tracking results compared with the high accuracy encoder. Furthermore, the MEMS-based angular acceleration estimation in particular is free from typical differentiation induced noise amplification and post-filtering phase-lag.**

I. Introduction

Hydraulic control systems suffer from inherent low system damping and thus an increase in damping is needed to allow a higher open-loop controller gain for high performance tracking control [1]. In servo-hydraulics, closed-loop pole placement is a well-established approach that requires full state feedback from actuator position, velocity and acceleration or a state observer design, see e.g. [2].

High accuracy and resolution joint position measurement is relatively straightforward with commercial contact-type angular sensors, such as magnetic or optical rotatory encoders that can easily provide accuracy of more than 1 arcsec. However, in addition to a high price, the drawback of this technology is two-folded. Firstly, these sensors require a mechanical contact interface to the manipulator rotating axles that is subject to wear and failures in harsh outdoor environments. Moreover, due to mechanical interface complexity and high precision mounting requirements, these sensors are costly to install to new manipulators joints and even more expensive to retro-fit into existing machines. Secondly, obtaining low-noise low-delay estimates of the joint angular velocities and angular accelerations is a less trivial task.

Whenever first and second order time derivatives of position are indirectly computed at high sampling rates using the traditional approach of single/double differentiation of position, or using predictive post-filtering on the differentiated signals, high-frequency perturbations and quantization effects are greatly amplified, e.g. [3]. Likewise, linear state observation and Kalman filter techniques avoid the need of differentiation but require system models to be available [4], [5], which may not be simple. Time-based encoder pulse counting techniques rely on high resolution time stamps to be available of encoder pulse count events, which typically leads to the use of external timer/counter hardware and increases the system cost further [6].

We consider full state feedback motion control of a heavy-duty hydraulic HIAB 031 manipulator, where micro-electro-mechanical systems (MEMS) components are utilized for a low-cost "strap-down" implementation. We will counter the aforementioned problems of indirect motion state estimation by applying a novel multi-MEMS configuration we have recently proposed in [7]. The axle-wise contact-free direct motion state sensing is founded solely on MEMS rate gyro and accelerometer readings, since metallic frames of many robotic manipulators make optional MEMS sensors such as magnetometers [8] often unusable. By geometrically modeling the linear and angular motion effects involved, we can reconstruct the HIAB 031 manipulator's "true" joint positions, angular velocities and angular accelerations directly without unwanted phase delay or distortion.

The focus of our paper is on manipulator vertical plane high-bandwidth motion control for analytical simplicity. To allow a fair performance verification, the developed MEMS-based state feedback controller is compared to state feedback control results obtained using highly accurate incremental encoder feedback with an angular resolution of 2×10^6 increments per revolution. Our robotic Cartesian space motion control experiments show that the dynamic response and path tracking performance of the cost-effective and easy-to install MEMS-based full state feedback controller is comparable to the high accuracy encoder results. Therefore, we consider the applied low-cost MEMS configuration promising and a significant step forward from our earlier motion control case [9], where a 1-DOF hydraulic mock-up was studied.

This paper is organized as follows. Sect. II provides the basis of the motion state estimation using MEMS components. Application of the estimated motion states in closed-loop state feedback control is also presented. Sect. III presents the experimental work, where our latest results concerning MEMS-based full motion state estimation of a multi-body linkage assembly in relatively fast motion are applied to the full state feedback control of full-size heavy-duty of HIAB 031 hydraulic manipulator. Finally, Sect. IV discusses the results and draws the relevant conclusions.

*This work was supported by the Academy of Finland under the project "Sensor Network Based Intelligent Condition Monitoring of Mobile Machinery", grant no. 133273.

[1]J. Honkakorpi and J. Mattila are with the Department of Intelligent Hydraulics and Automation, Tampere University of Technology, FI-33101, Finland. e-mail: firstname.surname@tut.fi

[2]J. Vihonen is with the Department of Signal Processing, Tampere University of Technology, FI-33101, Finland. e-mail: firstname.surname@tut.fi

II. Manipulator motion model and estimation

In this section, we provide a geometrical observational model for motion state estimation of a multi-body manipulator based on MEMS rate gyroscopes and linear accelerometers. The presented estimation approach is applicable to fully three-dimensional motion for a manipulator consisting of an arbitrary amount of rigid bodies. Then, the widely-applicable full state feedback motion control is also discussed briefly.

A. Direct manipulator motion state estimation using MEMS accelerometers and rate gyros

Consider an open-chain manipulator fixed to a base platform. Three-dimensional frames of rectangular (xyz) axes are attached to the center of each joint and the two links are directed along their y-axes. Let R_i denote the 3×3 body

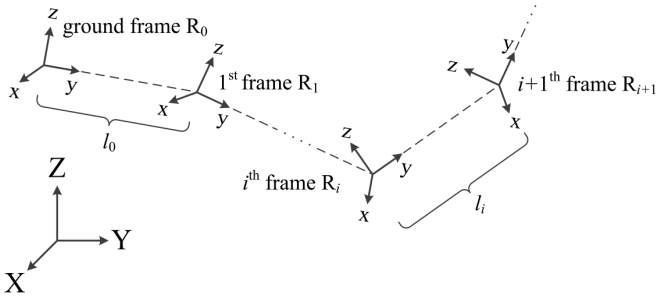

Fig. 1. Rigid body observation model

fixed rotation matrix, $\det(R_i)=1$ and $R_i^T=R_i^{-1}$, relating the i^{th} link frame to the inertial reference frame XYZ. The kinematic chain is illustrated in Fig. 1 where the lengths of the links are denoted by l_i.

The angular rate output of a MEMS gyroscope attached to the i^{th} link can be expressed as

$$\tilde{\Omega}_i = (I+S_i)\Omega_i + b_i + \mu_g \in \mathbb{R}^{3\times1}, \tag{1}$$

where Ω_i is the true rate value, I is the identity matrix, S_i is the scale factor error expressed as a percentage of Ω_i, b_i denotes a constant or slowly varying gyro bias, and μ_g denotes additive measurement noise. In view of the rigid body assumption, an estimate of the angular velocity of the i^{th} joint in Fig. 1 can be given by

$$\hat{\omega}_i = \tilde{\Omega}_i + \hat{b}_i - \sum_{m=0}^{i-1} R_i^T R_m \hat{\omega}_m \in \mathbb{R}^{3\times1} \tag{2}$$

denoting that the estimated joint angular rate $\hat{\omega}_i$ is the measured angular velocity of the i^{th} link $\tilde{\Omega}_i$, with the estimated angular velocities of each of the preceding joints subtracted from it. Note that we have introduced $\hat{b}_i$ to cancel the bias in $\tilde{\Omega}_i$.

The linear acceleration output of a MEMS accelerometer attached to the i^{th} link can be expressed as

$$a_i = (I+S_i)(v_i - R_i^T g) + b_a + \mu_a \in \mathbb{R}^{3\times1}, \tag{3}$$

where S_i is the scale factor error, g is the gravitational field $g=|g_0|e_3$, $|g_0|\approx9.8$ m/s^2, b_a is a bias term, and μ_a denotes additive measurement noise. Ideally, the instantaneous linear acceleration v_i can be given as

$$\begin{aligned} v_i &= \alpha_i \times d_i + \omega_i \times (\omega_i \times d_i) + \\ &\sum_{k=0}^{i-1} \Big((R_i^T R_k \alpha_k) \times d_k + \\ &\qquad (R_i^T R_k \omega_k) \times \big((R_i^T R_k \omega_k) \times d_k \big) \Big). \end{aligned} \tag{4}$$

where $\times$ denotes the cross product, α_i is the true angular acceleration of the i^{th} joint, ω_i is the true angular velocity of the i^{th} joint, the vectorial distance from the i^{th} joint rotation center is

$$d_i = [0\ p_i^y\ p_i^z]^T = p_i \tag{5}$$

and for the other rotation centers

$$d_k = R_i^T \sum_{m=k}^{i-1} R_m [0\ l_m\ 0]^T + d_i \tag{6}$$

for a low number of coordinate system transforms. If six linear accelerometers are attached to the i^{th} link (Fig. 2) and are organized into three pairs, we may write a direct estimate of the angular acceleration of the i^{th} joint as follows:

$$\hat{\alpha}_i = \begin{bmatrix} (a_i^{z_1} - a_i^z - \sigma_1^z)/d_i^{y_1} - \hat{\omega}_i^y \hat{\omega}_i^z \\ -(a_i^{z_2} - a_i^z - \sigma_2^z)/d_i^{x_2} + \hat{\omega}_i^x \hat{\omega}_i^z \\ (a_i^{y_2} - a_i^y - \sigma_2^y)/d_i^{x_2} - \hat{\omega}_i^x \hat{\omega}_i^y \end{bmatrix} \tag{7}$$

where the superscripts x, y, z denote the orthogonal sensing axes of the MEMS sensors on the i^{th} link. Here we account for the acceleration of the preceding joints according to (4) by calculating

$$\begin{aligned} \sigma_j &= \sum_{k=0}^{i-1} \Big(\big(R_i^T R_k \hat{\alpha}_k\big) \times (p_i^j - p_i) + \\ &\qquad \big(R_i^T R_k \hat{\omega}_k\big) \times \Big(\big(R_i^T R_k \hat{\omega}_k\big) \times (p_i^j - p_i) \Big) \Big) \end{aligned} \tag{8}$$

for a configuration of extra accelerometers positioned at

$$p_i^1 = p_i + \begin{bmatrix} 0 \\ d_i^{y_1} \\ 0 \end{bmatrix}, p_i^2 = p_i + \begin{bmatrix} d_i^{x_2} \\ 0 \\ 0 \end{bmatrix} \tag{9}$$

so that $d_i^{y_1}>0$ and $d_i^{x_2}\neq0$. By then computing an algebraic estimate of the instantaneous linear acceleration $\hat{v}_i$, we may estimate two degrees of freedom of the "true" link inclination rotation matrix R_i in fast accelerative motion since, for a triaxial accelerometer located at p_i, the above yields

$$a_i - \hat{v}_i \approx -R_i^T g. \tag{10}$$

Here the required estimates of angular velocity (2) and acceleration given by (7) can be obtained without complicated transforms. The configuration related to the estimates (2), (7), and (10), which are next used for closed-loop motion control of a heavy-duty hydraulic manipulator, is shown in Fig. 2.

The HIAB 031 manipulator with the MEMS configuration is shown in Fig 3, where the three estimated kinematic quantities are practically lag-free as no differentiation is

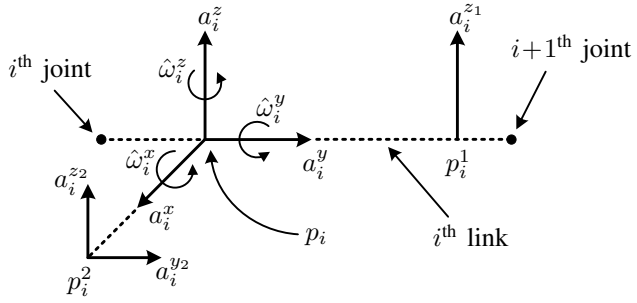

Fig. 2. A configuration of six linear accelerometers and a triaxial rate gyro attached to the i^{th} link. The extra single and biaxial accelerometers with their sensitive axes shown are used for direct angular acceleration sensing.

required. Note that because of low angular dynamics of the manipulator, the effects of the MEMS scale factor errors can be considered small. Under the rigid body assumption, real-time estimates of the joint angles can be given by

$$\hat{\phi}_i = \hat{\theta}_i - \hat{\theta}_{i-1}, \;\; i = 1, 2, \tag{11}$$

which denotes pair-wise subtraction of successive link inclination estimates $\hat{\theta}_i$ of the "true" rotation matrix R_i. The "ground" frame's rotation around x-axis is here simply included by using the horizontal position with respect to the gravity as our reference, i.e. $\hat{\theta}_0 = 0$ deg. High-bandwidth estimates of $\hat{\theta}_i$ are available by applying complementary and Kalman filtering to the accelerometer and gyroscope readings, please see [7] for further discussion.

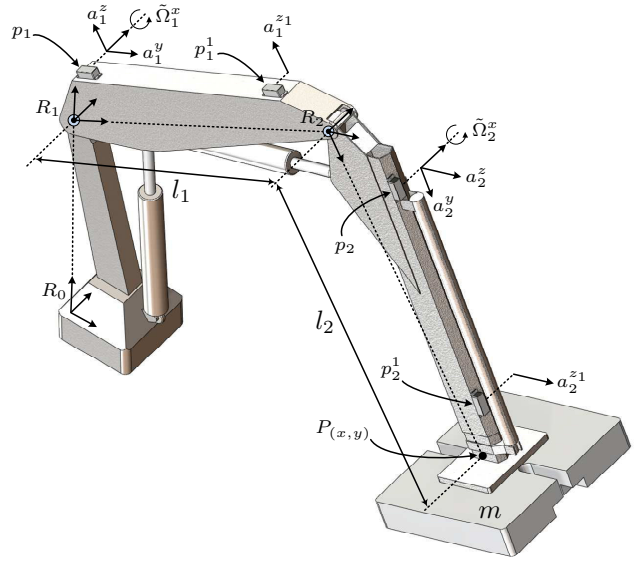

Fig. 3. MEMS sensor configuration on the hydraulic manipulator, $l_0 = 0\,\text{m}$ $l_1 = 1.6\,\text{m}, l_2 = 1.65\,\text{m}, m = 475\,\text{kg}$. For clarity, we assume the base platform's rotation $R_0 = I$, where I is the 3×3 identity matrix. The MEMS on the first link are located at points $p_1 = [0\ 0.21\ 0.23]^T$ m and $p_1^1 = [0\ 1.33\ 0.16]^T$ m respective to R_1. The MEMS on the second link are at points $p_2 = [0\ 0.24\ 0.22]^T$ m and $p_2^1 = [0\ 1.32\ 0.145]^T$ m respective to R_2. The initial inclination misalignment between the MEMS sensor orientations and the first link angle was 6.8 deg and 7.7 deg on the second link.

B. Hydraulic manipulator closed-loop state feedback control

Assuming a linear time-invariant system and treating all gravitational, inertial, centripetal and frictional terms as external disturbances, a hydraulic closed-loop position servo-system can be modeled with a linear second order transfer function between valve control input and joint velocity as

$$H(s) = \frac{V(s)}{U(s)} = \frac{K_{qa} \cdot \omega_n^2}{s^2 + 2\delta_n \omega_n s + \omega_n^2} \tag{12}$$

where $V(s)$ and $U(s)$ are the output velocity and control input, K_{qa} is the actuator velocity gain, δ_n is the natural damping ratio and ω_n is the natural frequency of the system [10]. A linear model of a full state feedback closed-loop control system can then be represented as shown in Fig. 4.

Although a simplification, the use of a linearized model is typically more relevant from the control perspective, since many applications of various control strategies rely on the use of a linear model. The control system consists of an inner second order velocity control loop with feedback gains K_v and K_a, an outer unity feedback, and a gain K_p for the position error. Incorporating the feedback gains K_v and K_a into the transfer function (12) the inner velocity control loop becomes

$$H_{vel}(s) = \frac{V(s)}{U(s)} = \frac{K_{qa} \cdot \omega_n^2}{s^2 + (2\delta_n \omega_n + K_a K_{qa} \omega_n^2)s + (1 + K_v K_{qa})\omega_n^2}. \tag{13}$$

Comparing transfer functions (12) and (13) we can see that the servo system with state feedback has a new damping ratio

$$\delta_n^{'} = \frac{2\delta_n + K_a K_{qa} \omega_n}{2\sqrt{1 + K_v K_{qa}}} \tag{14}$$

and a new natural frequency

$$\omega_n^{'} = \omega_n \sqrt{1 + K_v K_{qa}}. \tag{15}$$

From (14) and (15) it can be seen that the system damping increases with the acceleration feedback gain K_a. The natural frequency of the state feedback control system increases with the feedback gain K_v but at the same time, the damping ratio becomes smaller. Finally, the closed-loop transfer function from the reference position input $X(s)$ to the position output $Y(s)$ for the control loop in Fig. 4 is given by

$$H_{cl}(s) = \frac{Y(s)}{X(s)} \tag{16}$$

where $Y(s) = K_p K_{qa} \omega_n^2$

$$\text{and } X(s) = s^3 + (2\delta_n \omega_n + K_a K_{qa} \omega_n^2)s^2 + (\omega_n^2 + K_v K_{qa} \omega_n^2)s + K_p K_{qa} \omega_n^2.$$

In the experiments to follow the presented controller is applied individually to both joints of the manipulator and all coupling effects between the joints are seen as external disturbances to the joint controllers, which are not considered in this study.

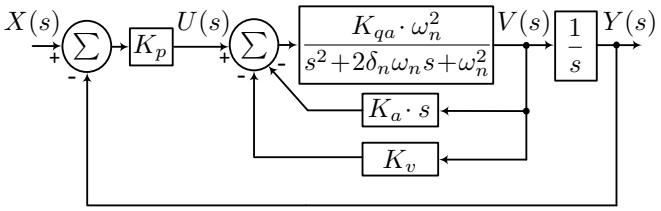

Fig. 4. State-feedback controller

Table I gives the system parameters for (12) that were experimentally identified for both joints in the operating region during the motion control experiments. The natural frequency was identified by observing the period of oscillation when the joints were controlled in open-loop and brought to a sudden halt. The natural damping ratio was identified from the decay rate of the oscillation.

TABLE I
MANIPULATOR SYSTEM PARAMETERS

	Joint1	Joint 2
ω_n (rad/s)	18	18
δ_n (-)	0.05	0.05
K_{qa} (rad/s)	1.3	1.9

III. EXPERIMENTS

The Cartesian trajectory motion control experiments with the MEMS-based closed-loop state feedback were performed on a HIAB 031 manipulator, which was installed on a rigid base as shown in Fig. 3. A load mass of 475 kg was attached to the end of the manipulator. The fluid flow to the lift and tilt cylinders, both ø80/45-545 mm in size, were controlled by directly operated NG10 size servo solenoid valves. The nominal flow rates of the valves controlling the lift and tilt cylinder were 100 l/min (Δp = 3.5 MPa per control notch). The bandwidth of the valves was 100 Hz for a $\pm 5\%$ control input. The hydraulic power supply was set to 19.0 MPa supply pressure. A PowerPC-based dSpace DS1103 system was used as a real-time control interface to the servo valves and for sampling of the joint sensors at a rate of 500 Hz (T_s = 0.002 s). The MEMS sensor chips are 8.5 $\times$ 18.7 $\times$ 4.5 mm in size containing a digital 3-axis $\pm 2g$ accelerometer integrated with a one x-axis $\pm$100 deg/s gyro by Murata [11]. The best case-inclination resolution of the MEMS accelerometer is $0.56 \cdot 10^{-3}$ rad when parallel to the ground. The MEMS gyro resolution is $0.35 \cdot 10^{-3}$ rad/s. The frequency range of the MEMS components is 30 Hz for the accelerometer and up to 50 Hz for the gyroscope.

In order to verify the developed MEMS-based closed-loop feedback performance, Heidenhain ROD 486 encoders outputting 5000 sine waves per revolution were also installed on the HIAB 031 manipulator to serve as high accuracy reference joint sensors. Connected to IVB 102 units for 100-fold interpolation and with each incremental pulse further sub-divided by 4 in the DS1103, the final encoder position resolution was $\pi \cdot 10^{-6}$ rad. Therefore, it can be concluded that the Heidenhain encoder reference sensors provide at least 100 times more accurate position feedback compared to the MEMS sensors. Interface to the MEMS sensor modules was through the CAN-bus operating at 1 Mbit/s.

To allow comparison of the MEMS-based state feedback control to encoder based state feedback, the joint velocity and acceleration were estimated from encoder feedback with a general finite difference method suited for real-time control applications (see [12]) defined as the discrete difference of the encoder position with respect to time t given by

$$\omega_i(t) \approx \frac{1}{T_s} \sum_{k=0}^{n-1} C_k \, \phi_i(t - k\,T_s) \tag{17}$$

where the weights $C = [5\ 3\ 1\ -1\ -3\ -5]/35$ yielded the best performance. The joint acceleration α_i was obtained by applying a second order difference operation to the encoder position given by

$$\alpha_i(t) \approx \frac{1}{T_s^2} \sum_{k=0}^{n-1} B_k \, \phi_i(t - k\,T_s) \tag{18}$$

where the weights are $B = [5\ -1\ -4\ -4\ -1\ 5]/28$.

As the rated frequency response of the MEMS components extends up to some 50 Hz, several higher frequency phenomena such as structural vibrations and pressure ripple in the fluid propagating from the hydraulic power unit are present in the accelerometer outputs. Considering the relatively low frequencies of motion of the hydraulic manipulator under study, these high frequency effects can be safely filtered from the angular acceleration feedback signals without causing control loop instability. For this task a geometric moving average (GMA) filter was used where the most recent input $u(k)$ is weighted by γ and past values are weighted by $(1 - \gamma)$. The filter is defined as a recursive equation

$$g_k = (1 - \gamma) g_{k-1} + \gamma\, u(k). \tag{19}$$

The value $\gamma = 0.04$ was experimentally identified to yield a suitable compromise between disturbance attenuation and low phase lag. To enable comparison, the same filter was also applied to the angular acceleration estimated from encoder position with (18). Figure 5 illustrates the resulting acceleration feedback signals when using encoder feedback or MEMS feedback. Additionally, an artificial dead-zone was introduced to the MEMS acceleration signal as the used hydraulic valve has a high bandwidth up to 100 Hz for a $\pm 5\%$ control input and thus the noise floor of the acceleration signal is translated into valve spool movement. The used angular acceleration dead-zone was set to $\pm$0.2 rad/s^2, which was also applied to the angular acceleration estimated from encoder position. These two techniques, the simple GMA noise suppression filtering and the introduction of an artificial dead zone, were found robust in our previous paper [9].

A. Position controller tuning

The state feedback controller can be designed using direct pole placement, deriving the gains from position control

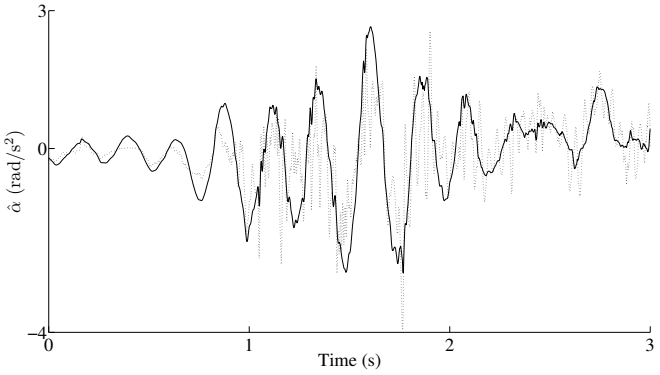

Fig. 5. Estimated angular acceleration $\hat{\alpha}$ during arbitrary motion using encoder feedback (dotted line) and MEMS feedback (black line).

settling time requirements or by using common criteria based on various error measurements between the desired and plant system model response e.g. ITAE. As the purpose of the experiments is to compare two different feedback schemes, specific controller performance criteria are not defined. The state controller gains K_p, K_v, and K_a were tuned iteratively by first finding the position gain value K_p where oscillation begins. Then the gain K_a was increased until the oscillation was removed. After this, the gain K_p can be increased again until the stability limit is reached. However, as shown in (14), the use of velocity feedback gain decreases the system damping and as the aim of this study is to increase the system damping and control the motion oscillations, the use K_v was omitted. The resulting controller gains are shown in Table II. Note that with MEMS acceleration feedback the gain $K_{a\,\text{mems}}$ is more than doubled compared to the encoder feedback. Although applying the optimal difference operator (18) and the GMA filter (19) the resulting encoder-based angular acceleration still contains large disturbances, as shown in Fig. 5, which limit the maximum stable value of $K_{a\,\text{enc}}$. In view of (14) the values in Table II yield new theoretical values for the natural damping ratios with MEMS feedback as $\delta_{n_1\,mems} \approx 0.64$ and $\delta_{n_2\,mems} \approx 0.39$. With encoder feedback the damping ratios are $\delta_{n_1\,enc} \approx 0.34$ and $\delta_{n_2\,enc} \approx 0.24$ for joints 1 and 2 respectively.

TABLE II
STATE FEEDBACK CONTROLLER GAINS

	K_p	K_v	$K_{a\,\text{enc}}$	$K_{a\,\text{mems}}$
Joint 1	15	0.0	0.025	0.05
Joint 2	10	0.0	0.011	0.02

To be able to determine the effectiveness of state feedback control, a proportional position controller was also implemented, where the controller structure is identical to that of Fig. 4 with the gains K_v and K_a set to zero. The maximum stable gain K_p for the proportional control was identified as $K_p = 5.75$ which was used for both joint controllers and both feedback cases.

B. Cartesian motion control experimental results

The position $P_{(x,y)}$ of the manipulator corresponding to given joint angles ϕ_1 and ϕ_2 can be obtained through forward kinematics by applying straightforward geometric principles. The resulting available manipulator workspace allowed by ϕ_1 and ϕ_2 is presented in Fig. 6 along with the Cartesian path used for the closed loop motion control experiments. The required manipulator joint angles for the point $P_{(x_d,y_d)}$ traveling along the illustrated path are determined using inverse kinematics in a similar geometric fashion.

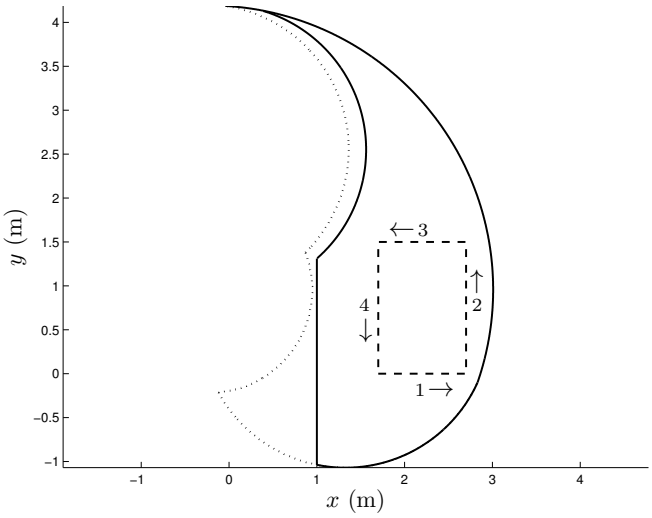

Fig. 6. HIAB 031 manipulator theoretical workspace (dotted line), available workspace with mass m attached (solid line), and driven Cartesian motion path (dashed line).

The path for the desired point $P_{(x_d,y_d)}$ for each line segment along the Cartesian path with respect to time t follows the fifth-order polynomial

$$x_d(t) = r_0^x + r_1^x t + r_2^x t^2 + r_3^x t^3 + r_4^x t^4 + r_5^x t^5 \quad (20)$$

$$y_d(t) = r_0^y + r_1^y t + r_2^y t^2 + r_3^y t^3 + r_4^y t^4 + r_5^y t^5 \quad (21)$$

which is a rest-to-rest type path (see e.g. [13]) i.e. with no acceleration at the rest points along the path. The polynomial coefficients r_i^x and r_i^y were recalculated to yield a desired path transition time of $t_d = 3.25$ s between each path segment. Figure 7 illustrates the resulting Cartesian velocities of the driven path when using proportional (P) control and state feedback control along with the desired velocity profile of the trajectory. The effect of the acceleration feedback is especially evident in the last segment of the path, where the considerable velocity oscillation is effectively dampened.

The path tracking accuracy of the control schemes can be evaluated using the distance

$$e_c = \sqrt{(x_d - x)^2 + (y_d - y)^2} \quad (22)$$

as the tracking error measurement, where x, y is the manipulator position calculated from the encoder joint position readings. The resulting dynamic path following errors are illustrated in Fig. 8. Note that despite the 100-fold advantage of the encoder in position resolution, the tracking

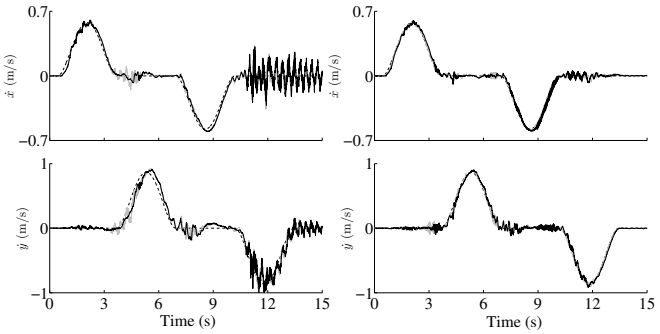

Fig. 7. Desired Cartesian path x and y velocity (dotted line) with estimated path velocities using P-control (left column) and state feedback control (right column). The feedback source was encoder (grey line) or MEMS (black line).

performance using MEMS position feedback is practically identical. Similarly with state feedback control the difference in tracking performance between the high accuracy encoder and the low-cost MEMS approach is very small with the MEMS feedback yielding occasionally even smaller errors.

Figures 9 and 10 illustrate the outputs of both P-control and state feedback control during the driven Cartesian path. In Fig. 9 the most notable difference between the feedback signals is the amount of noise in the encoder feedback compared with the MEMS acceleration estimates. With state feedback control (Fig. 10) the superior quality of the MEMS acceleration feedback and its effect on the controller is visible in the controller output signals particularly in the region around 6 seconds. Due to the differentiation operation the encoder acceleration noise is amplified greatly during periods of slow speeds and near-zero acceleration where the manipulator cylinder friction causes irregular movement. Furthermore, the level of disturbing accelerations during the driven motion path is generally lower with MEMS feedback.

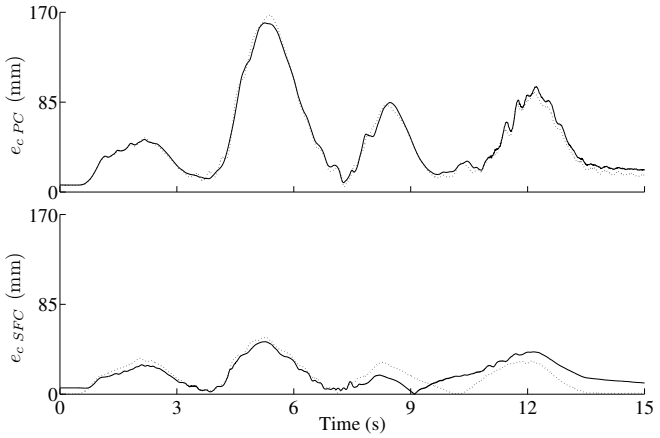

Fig. 8. P-control Cartesian path tracking error $e_{c\,PC}$ and state feedback control tracking error $e_{c\,SFC}$ using encoder feedback (dotted line) and MEMS feedback (black line).

IV. Discussion and Conclusion

In this paper multi-body motion state estimation based on low-cost MEMS linear accelerometers and rate gyros was applied to the closed-loop state feedback motion control of a heavy-duty hydraulic manipulator. The proposed estimation scheme of multi-MEMS accelerometer and gyro configuration was used for a high-bandwidth, low noise and low-phase lag estimation of the manipulator joint angles, angular velocities and angular accelerations. High resolution contact-type incremental encoders with 2 million increments per revolution were used as state estimation benchmark.

The use of state feedback control was motivated by the inherent poor damping qualities of the manipulator hydraulic control system. The effectiveness of state feedback control is evident in the Cartesian path tracking error, which was reduced up to 70% with state feedback control. Recalling Table II, using state feedback the position gain K_p can be increased considerably if compared with proportional position control, which enables a faster dynamic response and a better positioning accuracy. With the MEMS feedback the damping ratio of the hydraulic system was improved by a factor of 7-12. Due to the inferior quality of the encoder motion state feedback leading to smaller usable values of K_a, the damping ratio could only be improved by a factor of 5-7 when using encoder feedback.

As a key result, the tracking accuracy of manipulator position control by our low-cost contact-free MEMS motion estimation approach gives closely comparable results to that of using expensive high accuracy contact-type encoders. Combining a high controller sample rate necessary for acceleration-based feedback control with comparatively slow angular speeds of heavy-duty hydraulic manipulators, the motion states estimated from the encoder position contain significant noise and impulse-type perturbations.

Therefore, due to the relatively straightforward "strap-down" installation, immunity against local magnetic disturbances, size, cost and robustness advantage over the contact-type angular sensors, we consider our MEMS motion state estimation well applicable to the control of multi-body manipulators.

Acknowledgment

The authors wish to thank researchers Erkki Lehto and Janne Koivumäki from TUT/IHA for their valuable support with the MEMS electronics and experimental hydraulic manipulator setup design.

References

[1] R. Rahmfeld and M. Ivantysynova, "An overview about active oscillation damping of mobile machine structure," *Int. J. Fluid Power*, vol. 5, no. 2, pp. 5–25, 2004.

[2] R. Dorf and R. Bishop, *Modern Control Systems*, Pearson, Upper Saddle River, NJ, 2011.

[3] S. Ovaska and S. Väliviita, "Angular acceleration measurement: A review," in *Proc. of IEEE Instrum. and Meas. Tech. Conference*, 1998, pp. 875–880.

[4] A. Muhammad, J. Mattila, T. Virvalo, and M. Vilenius, "Improved positioning accuracy for a water hydraulic manipulator with state feedback controller," in *Service Robotics and Mechatronics*, pp. 347–352. Springer, 2010.

[5] Z. Jabbour, S. Moreau, A. Riwan, J. Van Rhijn, and G. Champenois, "Influence of speed estimation methods and encoder resolutions on the stiffness of a haptic interface," in *IEEE International Symposium on Industrial Electronics (ISIE)*, July 2010, pp. 1883–1888.

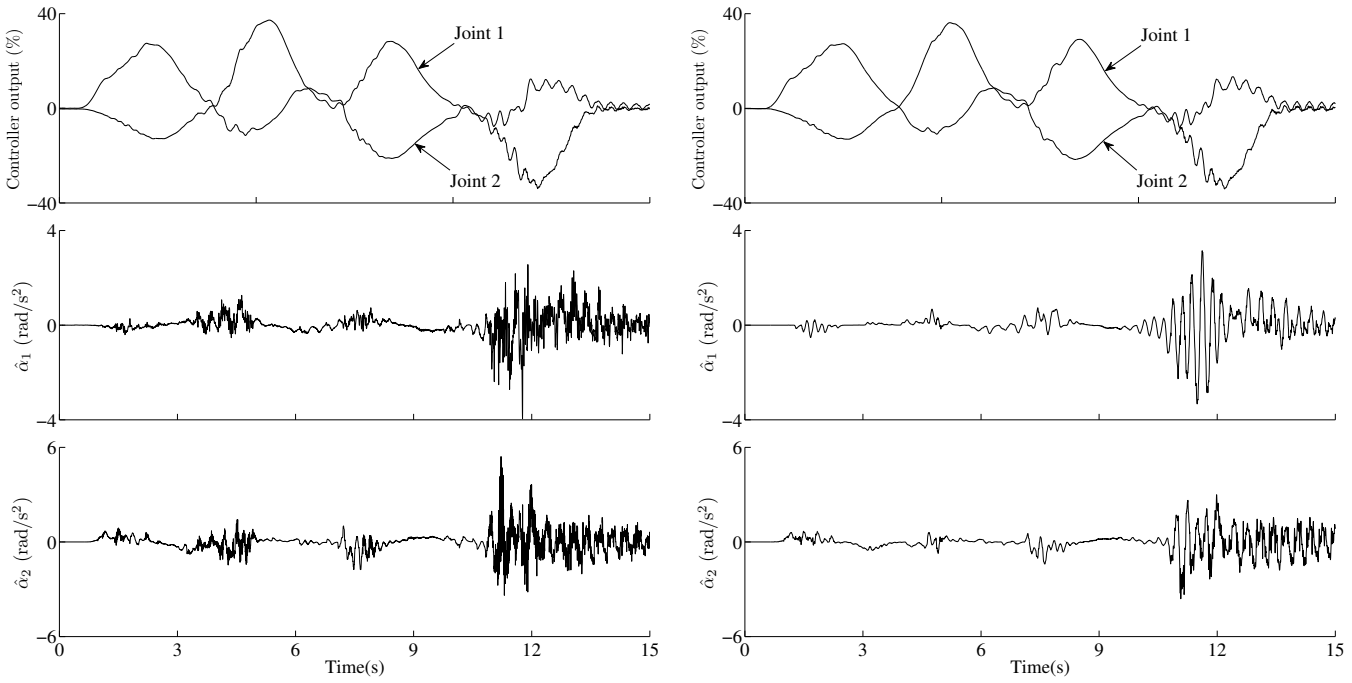

Fig. 9. Proportional position controller outputs and estimated joint accelerations $\hat{\alpha}_i$. Left column: feedback from encoder. Right column: feedback from MEMS.

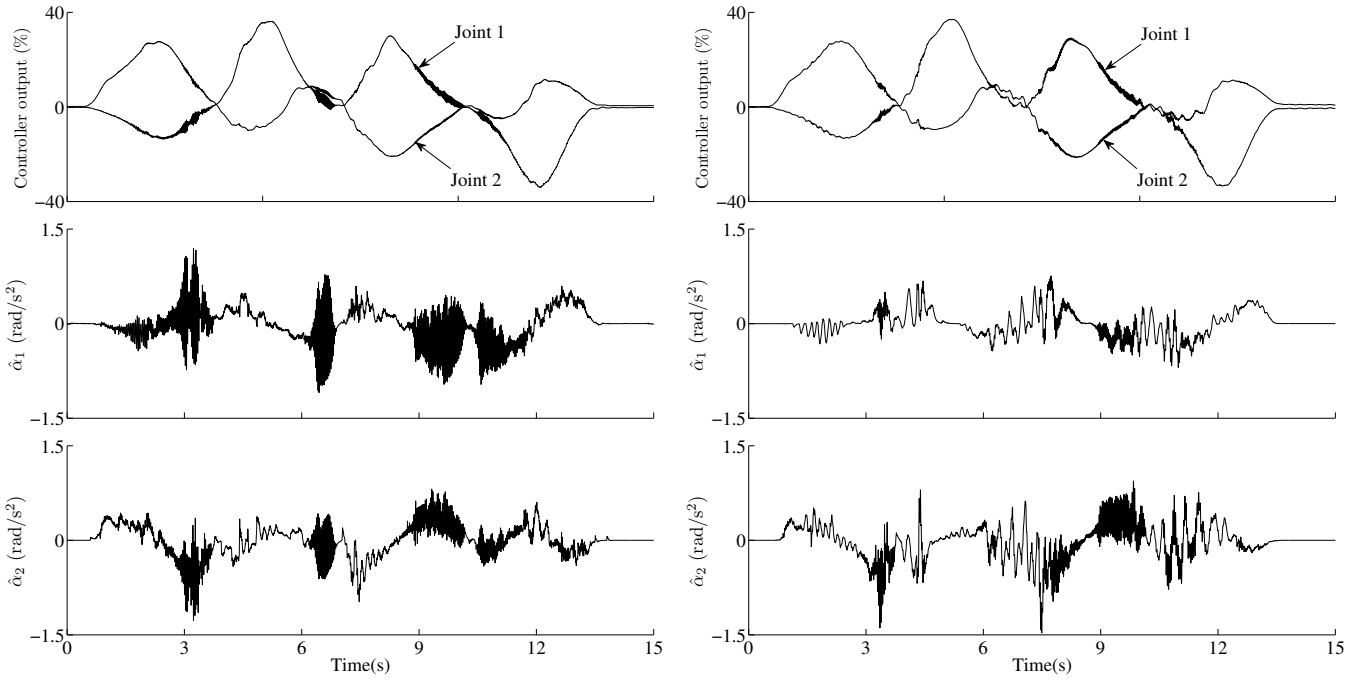

Fig. 10. State feedback controller outputs and estimated acceleration feedback signals $\hat{\alpha}_i$. Left column: using encoder feedback. Right column: using MEMS feedback.

[6] R. J. E. Merry, M. J. G. van de Molengraft, and M. Steinbuch, "Velocity and acceleration estimation for optical incremental encoders," *Mechatronics*, vol. 20, no. 1, pp. 20–26, Feb. 2010.

[7] J. Vihonen, J. Honkakorpi, J. Mattila, and A. Visa, "Geometry-aided angular acceleration sensing of rigid multi-body manipulator using mems rate gyros and linear accelerometers," in *IEEE/RSJ Int. Conf. on Intelligent Robots and Systems (IROS)*, Tokyo, Japan, Nov. 2013, accepted for publication.

[8] M. J. Caruso, "Applications of magnetic sensors for low cost compass systems," in *IEEE Pos. Loc. and Nav. Symp.*, Aug. 2000, pp. 177–184.

[9] J. Honkakorpi, J. Vihonen, and J. Mattila, "Sensor module for hydraulic boom state feedback control," *Int. J. Fluid Power*, vol. 13, no. 3, pp. 15–23, Nov. 2012.

[10] J. Watton, *Fluid Power Systems : modelling, simulation, analog and microcomputer control*, Prentice Hall, New York, 1989.

[11] Murata Electronics Oy, "SCC1300-D02 combined x-axis gyroscope and 3-axis accelerometer with digital SPI interfaces," www.muratamems.fi, Aug. 2012.

[12] A. J. L. Harrison and D. P. Stoten, "Generalized finite difference methods for optimal estimation of derivatives in real-time control problems," *Proc. Instn. Mech. Engrs.*, vol. 209, no. 2, pp. 67–78, May 1995.

[13] Reza N. Jazar, *Theory of Applied Robotics: Kinematics, Dynamics, and Control*, Springer, 2nd edition, 2010.